Class I Phospho-inositide-3-kinases (PI3Ks) Isoform-Specific Inhibition Study by the Combination of Docking and Molecular Dynamics Simulation

Ming Han*,† and John Z. H. Zhang‡,§

Institute of Theoretical and Computational Chemistry, Key Laboratory of Mesoscopic Chemistry of MOE, School of Chemistry and Chemical Engineering, Nanjing University, Nanjing 210093, China, State Key Laboratory of Precision Spectroscopy, Department of Physics, East China Normal University, Shanghai 200062, China, and Department of Chemistry, New York University, New York, New York 10003

Received May 13, 2009

The combination of docking and molecular dynamics simulation is used to explain the isoform-specific selectivity between PI3Kα and PI3Kγ, which are two lipid kinases in the class I PI3Ks. The protein flexibility is incorporated in docking the ligands to the ensemble of representative structures extracted from a clustering analysis of the molecular dynamics simulation in explicit aqueous solution. The reported most potent PI3Kα inhibitor PIK-75 was studied, and we predicted three possible PIK-75-bound conformations for PI3Kα and two for PI3Kγ. Comparative analysis between the PI3Kα and PI3Kγ docking experiments indicates that the residue Trp780 and Asn782 in PI3Kα and the corresponding residues Trp812 and Glu814 in PI3Kγ in the solvent-accessible region can confer the PI3Kα and PI3Kγ isoform specificity. The predicted bound conformations are further studied in aqueous solution by molecular dynamics simulation. The work provides a possible effective pharmacophore model for PI3Kα inhibitor. The dynamic behaviors of the LY294002-bound PI3Ks are studied too.

1. INTRODUCTION

Phosphatidyl-inositol-3-kinases (PI3Ks) are a lipid kinase family that plays an important role in signal transduction.[1,2] Activated by upstream signaling events, the class I PI3K can convert the membrane lipid phosphatidylinositol 4,5-biphosphate, also called PIP_2, to phosphatidylinositol 3,4,5-trisphosphate (PIP_3), which distinguishes the class I PI3Ks from other subfamilies of PI3Ks.[3] PIP_3 is an important second messenger molecule that activates protein kinase B (PKB) in the PI3K signaling pathway. The activated PKB will turn on the signaling cascades, leading to cell proliferation, survival, and cell growth.[4] Class I PI3Ks include four isoforms consisting of two subdivisions, namely, class IA (PI3Kα, -β, -δ) activated by tyrosine kinases, antigen and cytokine receptors, and class IB (PI3Kγ) activated by G-protein-coupled receptors.[5,6] PI3K enzymes play an important part in cancers.[7−10] In particular, the PIK3CA gene (which encodes p110α, the catalytic subunit of PI3Kα) is somatically mutated at high frequency, and the mutations in the catalytic domain constitutively confer a marked increase in its kinase activity.[11,12] Therefore, the oncoproteins of PI3Ks have become an important target for the development of small molecule inhibitors.[13]

Developing potent and isoform-specific small molecule inhibitors against the PI3K lipid kinases that minimize the undesirable medical side effects remains a significant challenge. The very conserved kinase binding site has high sequence similarity. Moreover, the disclosed SAR homology by real experiments, that is, among the class I PI3Ks, inhibitors of PI3Kβ often potently inhibit PI3Kδ, whereas inhibitors of PI3Kα often potently inhibit PI3Kγ,[14] makes it more challenging to find inhibitors with high selectivity between PI3Kβ and PI3Kδ or between PI3Kα and PI3Kγ. Thus, most of the compounds characterized are not specific and inhibit other PI3Ks as well as other kinases.[15] Are the class I PI3Ks too similar to find an isoform-specific inhibitor or is there still a chance to identify the molecules that display high selectivity among the isoforms in class I PI3Ks especially between PI3Kα and PI3Kγ or between PI3Kβ and PI3Kδ?

In this work we concentrate on understanding the isoform-specific inhibition profile between PI3Kα and PI3Kγ. The p110α and p110γ isoforms share ∼35% sequence identity, and the kinase domain sequence identity is ∼43.5%. Several studies based on crystal structures or homology models have been conducted.[16−18] Amzel et al.[16] compared the X-ray crystal structures of PI3Kα and PI3Kγ and speculated that the different conformations of the loops containing residues 771−779 chould be exploited for the design of the isoform-specific PIK-39 inhibitors. In Zvelebil et al.'s work[17] His855 and Gln859 are suggested to confer the inhibition specificity to PIK-39. The homology model and docking work from Frédérick and Denny[18] indicate that His855 and Ser773 residues might account for the PIK-75 selectivity profile within PI3K isoforms. All these studies are based on one conformation from the X-ray structure or one homology model. However, protein flexibility plays an important role in molecular recognition. Recently, methods have been developed to incorporate receptor flexibility in structure-based drug discovery.[19−26] In our study, we take into account the full receptor flexibility by the combination of docking

* Corresponding author e-mail: minghan2000@gmail.com.
† Nanjing University.
‡ East China Normal University.
§ New York University.

10.1021/ci900175n
Published on Web 11/20/2009

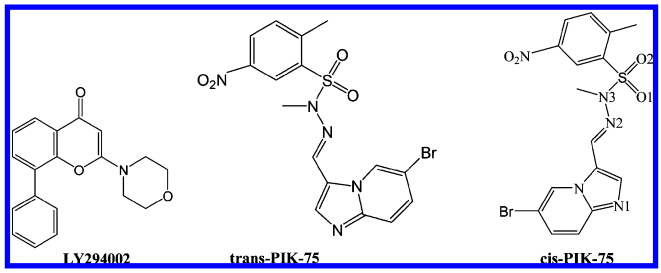

Figure 1. Chemical structures of LY294002, *trans*-PIK-75, and *cis*-PIK-75.

and molecular dynamics simulation (MD) methods to try to discover the reason for the isoform specificity between the PI3Kα and the PI3Kγ structures. Structures of several inhibitor-bound PI3Kγ[14,27,28] and the recent PI3Kα apo X-ray structure (PDB code 2RD0)[29] have been reported, which makes our work possible. The inhibitor that shows selectivity between PI3Kα and PI3Kγ, imidazo[1,2-*a*]pyridine derivative PIK-75[14,30] (shown in Figure 1), is mainly studied.

2. METHODS AND COMPUTATIONAL DETAILS

There are three main steps in our calculation work. First, docking experiments were performed for LY294002 and PIK-75 to PI3Kα and PI3Kγ crystal structures. The orientation of the docked LY294002 is consistent with the docked LY294002 in the PDB structure of 1E7V.[27] However, PIK-75 failed in docking to PI3Ks X-ray structures correctly. Ten nanosecond molecular dynamics simulations of LY294002-bound PI3Kα and PI3Kγ were run to extract representative conformations in order to consider the flexibility of the receptor. Second, PIK-75 was docked to the ensemble of the representative PI3Kα and PI3Kγ structures. Third, the stability of the predicted poses was studied in explicit aqueous solution. The receptor and ligand preparation and the methods used in the calculation are listed as follows.

2.1. Receptor and Ligand Preparation. The initial models come from the X-ray solved crystal structure of apo PI3Kα (PDB code 2RD0)[29] and pyrazolopyrimidine-S2-bound human PI3Kγ (PDB code 3ENE).[28] The kinase domains were truncated from Met697 to Lys1063 for PI3Kα and Thr726 to Leu1092 for PI3Kγ. Residues 941−950 of the activation loop, residues beyond 1050 of the PI3Kα, as well as residues 969−978 of PI3Kγ were disordered and not traced. The lost loop zones of the two X-ray structures were generated and refined by ab initio refinement of the loop in the loop refine module of Modeler 9v5.[31,32] Residues beyond 1050 of PI3Kα were generated based on the template of the PI3Kγ structure. In our calculation, all of the ionizable residues are in the ionization states expected at pH 7 based on the standard pK_a values. Two isomers of the PIK-75 shown in Figure 1 are considered in our docking. The chirality from the nitrogen atom nearest to the sulfonyl group does not affect the final docking results significantly. Ligands were built and optimized by the Gaussian 03 package[33] at the DFT/B3LYP/6-31G* level. When we talk about PI3Kα and PI3Kγ in the following part we refer to the truncated kinase domains of the proteins.

2.2. Docking Experiments. AutoGrid 4.0[34,35] was used to create affinity grids centered on the active site with 126 × 126 × 126 grid size with a spacing of 0.2 Å. AutoDockTools-1.5.4[36] was used to merge nonpolar hydrogens, set up rotatable bonds, and add charges to each ligand. The topology-dependent Gasteiger charge[37] was used to assign charges to the protein and ligands for convenience to take into account the flexibility of the protein and ligand. The rigid kinase receptors and flexible ligands dockings were performed by using AutoDock 4.0[34,35] with the Lamarckian genetic algorithm applying the following protocol: trials of 100 dockings, energy evaluations of 25 000 000, population size of 200, a mutation rate of 0.02, a crossover rate of 0.8, and an elitism value of 1. In the Lamarckian genetic algorithm dockings, the pseudo-Solis and Wets local search method was used. The docking results were evaluated by sorting the binding free energy predicted by docking conformations. Docked conformations were clustered using a tolerance of 1.5 Å rmsd. The standard error allowed in AutoDock is ∼2.1 kcal mol^{-1}. The single-point energy analysis was calculated by AutoDockTools-1.5.4.

2.3. Molecular Dynamics Simulation. The solvation, molecular dynamics simulations, and clustering were run using AMBER10.[38] Sodium ions were added to the system by random replacement of water molecules until neutrality was achieved. The numbers of water molecules, ions, total atoms, periodic image distance, as well as total simulation time in each simulated system are listed in Table 1. Box volume is given by $(4)/(9)\sqrt{3}d^3$, where d is the periodic image distance for an octahedron. We select the Amber99SB[39] force field for proteins and Amber GAFF parameters[40] for ligands. The atomic charges and atom types are assigned by the antechamber tool in the Amber software package. The less conformational-dependent charge distribution AM1-BCC model[41,42] is used for our predicted drug−kinase complexes. The atomic types and partial atomic charges of the ligands are available in the Supporting Information. The missing force field parameters for LY294002 and PIK-75 are listed in the Supporting Information too. Other force field parameters can be found in gaff.dat in the Amber software package.

TIP3P water was used to solvate the system as an octagonal box. The calculation of electrostatic forces utilized the PME implementation of the Ewald summation method.[43] A cutoff of 8 Å was used for the van der Waals interactions. Energy minimizations were performed employing a steepest descent algorithm following the setup to relax any steric conflicts generated during system setup. The system was then subjected to a restrained MD run for 500 ps. In the first 100 ps the system was heated from 0 to 300 K. The non-hydrogen protein atoms were restrained with a force constant of 2 kcal mol^{-1} Å^{-2} to enable the water to pack properly around the protein. The production simulations were run in the NPT ensemble, and the temperature was coupled by using a Langevin thermostat[44,45] at 300 K, with a collision frequency of 2.0 ps^{-1}. System pressures were isotropically coupled using the Berendsen method[46] at 1 bar via a coupling constant of 2.0 ps. The bonds of nonwater molecules and water molecules are constrained by using the SHAKE[47] and SETTLE[48] algorithms, respectively. The integration time step was 2 fs, and the coordinates and velocities were saved every 4 ps for subsequent analysis. Other data were analyzed by AMBER10 or locally written codes.

2.4. Clustering Molecular Dynamics Trajectories. The average-linkage clustering and K-means clustering algorithms

Table 1. System Composition, Periodic Image Distance, and Simulation Time in Each MD Simulation System

receptor	ligand	water number	Na^+ number	total number of atoms	periodic image distance (nm)	simulation time (ps)
PI3Kα	LY294002	14 046	0	48 201	8.91596654	10 000
PI3Kγ	LY294002	12 756	5	44 214	8.67924390	10 000
PI3Kα	PIK-75 pose α_A	14 331	0	49 057	8.98044898	10 000
PI3Kα	PIK-75 pose α_B	14 371	0	49 177	8.99112340	5000
PI3Kα	PIK-75 pose α_C	14 377	0	49 195	8.99155629	5000
PI3Kγ	PIK-75 pose γ_A	13 190	5	45 517	8.78019109	5000
PI3Kγ	PIK-75 pose γ_B	13 173	5	45 466	8.77654316	5000

Table 2. PI3Kα and PI3Kγ Selectivity for PIK-75 in Comparison with LY294002 and the Binding Free Energy from Experiment

ligand	IC_{50}_PI3Kα (μM)	binding free energy (kcal mol^{-1})	IC_{50}_PI3Kγ (μM)	binding free energy (kcal mol^{-1})
LY294002	9.3	−6.86353	38	−6.02965
PIK-75[14]	0.0058	−11.23556	0.076	−9.71133
PIK-75[30]	0.0003	−12.99022	0.040	−10.09158

were used to generate representative structures from molecular dynamics simulations. Receptors were extracted at 20 ps intervals over the 10 ns simulation. The rmsd clustering was performed on the subset of residues within 15 Å around the ATP-binding site.[49] The centroid, the structure within the cluster having the smallest rmsd to all other structures within the cluster, was chosen as the cluster representative structure. The energy of the representative conformations were minimized before docking experiments.

Structural diagrams were prepared by using PyMol 0.99rc6.[50]

3. RESULTS AND DISCUSSION

Like other typical kinases, the PI3K kinase domain consists of a mostly α-helical carboxy-terminal (C−) lobe and an amino-terminal (N−) lobe between which the ATP binding pocket is located. All known PI3K inhibitors make backbone hydrogen-bond interactions with the hinge region, which is the short polypeptide connecting the C- and N-terminal lobes, and have extensive hydrophobic contacts with the residues around the adenine-binding region.[14,27,51] Therefore, in our docking experiments, we define the poses with the hydrogen bond between the nitrogen atom of the imidazole and the backbone of the hinge region as the correct poses. The poses lacking the critical hydrogen-bonding interaction with Val851 in PI3Kα or Val882 in PI3Kγ are not considered for further analysis.

The small molecule ATP-competitive inhibitor LY294002 is a pan-PI3K inhibitor that has only micromolar affinity with PI3Ks. PIK-75 is the most potent specific PI3Kα inhibitor reported to date. The experimental IC_{50} values of LY294002 and PIK-75 are summarized in Table 2. The Gibbs binding free energy, ΔG, is determined by using the equation $\Delta G = RT \ln K_i$, where R is the gas constant and T is the absolute temperature. The inhibition constant K_i can be obtained from the IC_{50} value using the Cheng−Prusoff equation:[52] $K_i = IC_{50}/(1 + [S]/K_m)$, where K_m is the Michaelis affinity constant of the substrate for the enzyme and [S] is the substrate concentration. IC_{50} approaches K_i when the substrate concentration is significantly lower than K_m. In Knight et al.'s work[14] PIK-75 inhibits PI3Kα and PI3Kγ with IC_{50} values of 0.0058 and 0.076 μM, respectively, whereas in Hayakawa et al.'s work[30] the IC_{50} values are 0.0003 and 0.040 μM. While the reason for the differing absolute IC_{50} values is not clear, it could be related to slight differences in assay methodologies or in the source of the enzyme.[53]

3.1. Docking LY294002 and PIK-75 to Apo Crystal Structures of PI3Kα and PI3Kγ. No inhibitor-bound PI3Kα crystal has been solved yet; therefore, we applied docking experiments to obtain the inhibitor-bound complex for further study. In our docking experiment, LY294002 docked to PI3Kα and PI3Kγ structures in a manner identical to that in PDB 1E7V[27] and dockings converged to only one cluster. However, PIK-75 failed in binding to the X-ray structure of both PI3Kγ and PI3Kα correctly. Possible explanations for the incorrect docking include the apo structure of PI3Kα as well as the 3.0 Å resolution of the X-ray structure. Thus, we try to extract representative conformations from the molecular dynamics simulation of LY294002-bound PI3Ks to consider the flexibility of the receptor.

3.2. Molecular Dynamics Simulation of LY294002-Bound PI3Kα and LY294002-Bound PI3Kγ. Molecular dynamics simulations for both LY294002-bound PI3Kα and LY294002-bound PI3Kγ in explicit aqueous solution were run for a duration of 10 ns. The system composition, periodic image distance, as well as total simulation time in each simulated system, are listed in Table 1. The simulations reached equilibrium within 4 ns. The rmsd from the starting structure was analyzed as a function of time to assess the degree of conformational drift, as shown in Figure 2. As can be seen in the plots, the receptor and ligands in both PI3Kα and PI3Kγ are stable after equilibrium. The ∼1 Å fluctuation of the rmsd of LY294002 in the beginning of the simulation of LY294002-bound PI3Kα comes from rotation of the bond between the two benzene rings.

The hydrogen bonds in the ATP-binding pocket play a key role in kinase function and drug inhibition. The important residues involved in the key hydrogen bonds in the ATP pocket are listed in Table 3 and shown in Figure 3. Figure 3 includes the sixth representative conformation of PI3Kα and third cluster representative conformation of PI3Kγ by the average-linkage clustering algorithm, which we will discuss further in section 3.3. The hydrogen-bond occupancy of the key hydrogen bonds of PI3Kα was analyzed as a function of the simulation time as shown in Figure 4. The simulation time is divided into 50 intervals of 200 ps. We calculate the hydrogen-bond occupancy in each interval. A hydrogen-bond occupancy of greater than 100% means there is more than one hydrogen bond between the two studied residues. In the simulation of LY294002-bound PI3Kα, Asp805 formed stable hydrogen bonds with Lys802 and Lys776. Asp933 formed a stable hydrogen bond with

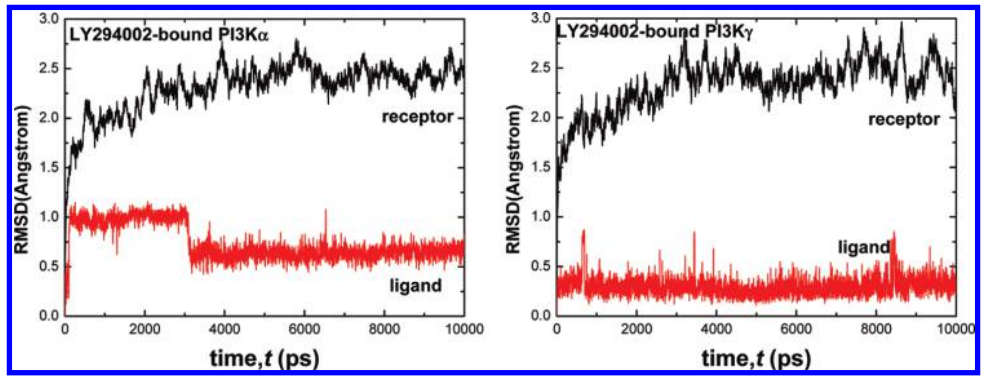

Figure 2. rmsd of Cα of the receptor and the heavy atoms in the ligand (black and red lines, respectively) of LY294002-bound PI3Kα- (left) and LY294002-bound PI3Kγ (right) as a function of the simulation time.

Table 3. Residues Involved in Key Hydrogen Bonds That Line in the ATP Binding Pocket

PI3Kα	Ala775	Lys776	Lys802	Asp805	Asp810	Asp933	Ser919	Trp780	Asn782
PI3Kγ	Lys807	Lys808	Lys833	Asp836	Asp841	Asp964	Asp950	Trp812	Glu814

Lys776, but it lost the stability in the last 2 ns. The hydrogen bond between Asp810 and Lys802 formed just occasionally.

The hydrogen-bond occupancy analysis for LY294002-bound PI3Kγ is shown in Figure 4 too. The hydrogen bonds between Asp841 and Lys833, between Asp836 and Lys808, and between Asp964 and Lys833 were stable in the simulation. Lys807 has hydrogen bonds with Asp964 and Asp950 in the initial structure, but the hydrogen bond broke shortly after the simulation began. Lys807 was observed to leave Asp964 and Asp950 and finally was solvated by bulk water molecules in the trajectory. We simulated the ligand-free p100γ (the catalytic subunit of PI3Kγ, unpublished data) and found the hydrogen bonds from the X-ray structures were stable. This difference may result from the inhibitor-bound complex structure, high flexibility of the P-loop, or the simulation force field. More study is required to investigate the reason. In PI3Kα, Ala775, and Ser919, the equivalent residues at these positions for Lys807 and Asp950 in PI3Kγ, have no chance to form a hydrogen bond. Asp836 and Lys833 in PI3Kγ formed a hydrogen bond occasionally.

3.3. Docking PIK-75 to the Ensemble of the Representative PI3Kα and PI3Kγ Structures. *3.3.1. Cluster Representative PI3Kα and PI3Kγ Structures.* To account for the receptor flexibility in the ligand binding, representative structures were extracted from a clustering analysis of the 10 ns molecular dynamics simulation of LY294002-bound PI3Kα and LY294002-bound PI3Kγ by the average-linkage and K-means clustering algorithm. Six clusters were obtained by the average-linkage clustering algorithm and five clusters by the K-means clustering algorithm for both PI3Kα and PI3Kγ. All snapshots in each cluster form a continuous portion of the trajectory by two algorithms as the cluster distribution is shown in Figure 5. The first clusters extracted by the average-linkage clustering algorithm have few snapshots and will not be considered in the following calculation.

The representative conformations of PI3Kα extracted by the average-linkage clustering algorithm are superimposed onto the apo X-ray structure by the sequence alignment as shown in Figure 6. The rmsd of the Cα atom of the whole protein to the reference protein is 2.07, 2.21, 2.62, 2.29, and 2.41 Å for the five representative structures, respectively. The P-loop at the active site cleft shows significant conformational flexibility. The rmsd of the Cα atom of the P-loop (residues 771−779) of the protein to the P-loop of the reference protein is as big as 2.89, 3.56, 4.10, 3.71, and 2.44 Å for the five representative structures, respectively. The P-loop in the apo structure adopts a more open conformation than that in other representative conformations, which agrees with the knowledge that the ligand-free structures are in the most open form. An obvious difference between the representative structure of the sixth cluster and the others is the hydrogen bond between Asp933 and Lys776. As shown in Figure 4, this hydrogen bond is unstable in the last 2 ns of the simulation of the LY294002-bound PI3Kα. Thus, the hydrogen bond does not happen in the representative structure of the sixth cluster as shown in Figure 3. The

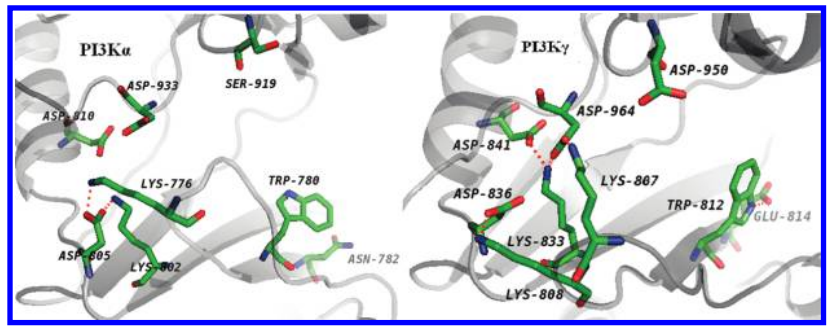

Figure 3. View of the key hydrogen-bond interactions among the residues in the pocket domain of PI3Kα (left) and PI3Kγ (right). Green, red, and blue represent carbon, oxygen, and nitrogen, respectively. Hydrogen bonds are red dashes. The two structures are the representative structures from the sixth cluster of PI3Kα and the third cluster of PI3Kγ calculated by the average-linkage clustering algorithm.

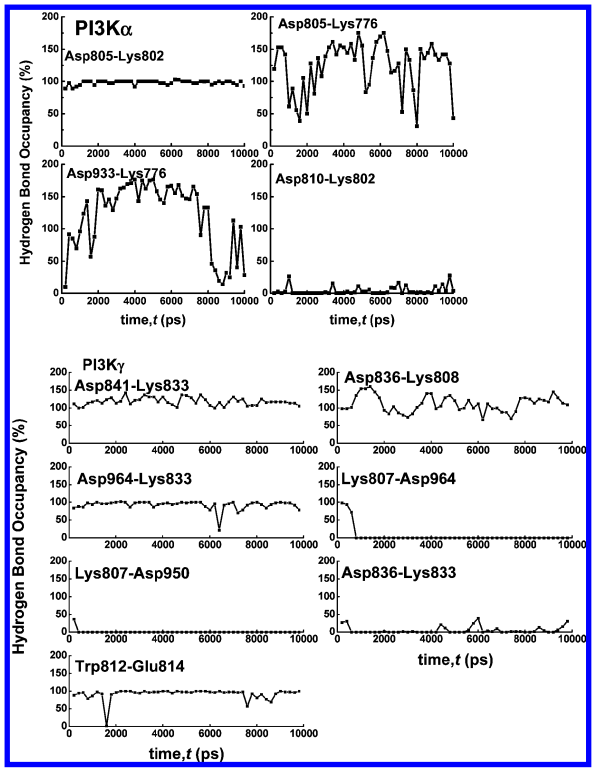

Figure 4. Hydrogen-bond occupancy analysis along the simulation time for the residues around the ATP binding pocket of PI3Kα and PI3Kγ.

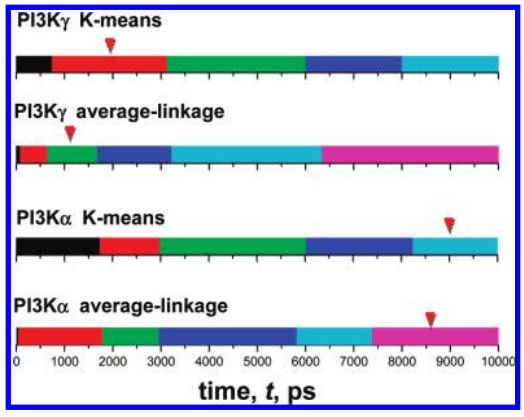

Figure 5. Molecular dynamics simulation trajectories cluster distribution along the simulation time. Black, red, green, blue, cyan, and purple are for the first, second, third, fourth, fifth, and sixth cluster, respectively. The red triangle indicates the clusters that get the best docking results.

superimposed representative conformations of PI3Kγ are shown in Figure 6. The rmsd of the Cα atom to the reference X-ray structure is 1.98, 1.91, 1.95, 1.87, and 1.93 Å for the five representative structures, respectively. The five representative structures are superimposed very well with a small rmsd difference, which can be observed from the loops, especially in the P-loop. The rmsd of the Cα atom of the P-loop (residues 803−811) of the protein to the P-loop of the reference protein is as small as 1.32, 1.61, 1.41, 1.37, and 1.62 Å for the five representative structures, respectively. The smaller rmsd fluctuation compared with the PI3Kα structures results from the high-resolution holo X-ray structure.

3.3.2. Result of Docking PIK-75 to the Ensemble of the Cluster Representative Structures. The *cis*- and *trans*-isomers of PIK-75 were docked to 10 representative conformations

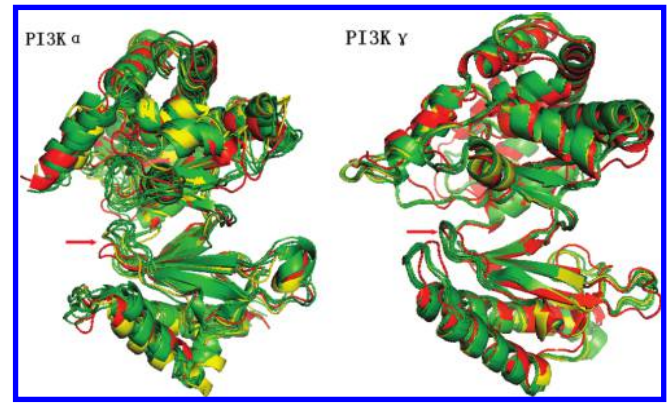

Figure 6. (Left) Five representative structures from clustering the molecular dynamics simulation of LY294002-bound PI3Kα by the average-linkage clustering algorithm superimposed onto the apo X-ray structure of PI3Kα (red). The representative structure from the sixth cluster of PI3Kα is represented by yellow. Other conformations are shown in green. (Right) Five representative structures from clustering the molecular dynamics simulation of LY294002-bound PI3Kγ by the average-linkage clustering algorithm superimposed onto the X-ray structure of PI3Kγ (red). The representative structure from the third cluster of PI3Kγ is represented by yellow. Other conformations are shown in green. The red arrow points to the P-loop that connects kβ3 and kβ4.

of PI3Kα and 10 representative conformations of PI3Kγ. The docking results were sorted by the binding free energy, and only the correct hits were chosen for further analysis. The two most successful docking results for PI3Kα are shown in Figure S3, Supporting Information. The best docking took place when the *cis*-isomer was docked to the sixth cluster representative conformation, which accounts for 26.2% of the ensemble of PI3Kα as calculated by the average-linkage clustering algorithm, and to the fifth cluster representative conformation, which accounts for 17.6% of the ensemble of PI3Kα as computed by the K-means clustering algorithm. The most populated cluster includes more than 50% of all docked conformations. Because all snapshots of each cluster form a continuous portion of the trajectory by the two algorithms, it is reasonable that both best docking experiments took place in the last cluster. The three most populated clusters for the two most successful docking experiments predicted the poses of PIK-75 with the same or a very similar spatial orientation. The docking experiments to other representative structures failed because no critical hydrogen bonds were formed or the population was too small. This is further evidence that the docking result is very sensitive to the conformation of the receptor, and it is necessary to develop the docking method to consider the receptor flexibility. We refer to the three structures with three poses of PIK-75 in the top three ranked clusters as pose α_A, pose α_B, and pose α_C.

The two most successful docking results for PI3Kγ are shown in Figure S4, Supporting Information. The best docking took place when the *cis*-isoformer of PIK-75 was docked to the third cluster representative conformation, which accounts for 10.4% of the ensemble of PI3Kγ as calculated by the average-linkage clustering algorithm, and the second cluster representative conformation, which accounts for 23.8% of the ensemble of PI3Kγ as computed by the K-means clustering algorithm as shown in Figure S4, Supporting Information. The two lowest-energy clusters are less populated than the other clusters with higher energy.

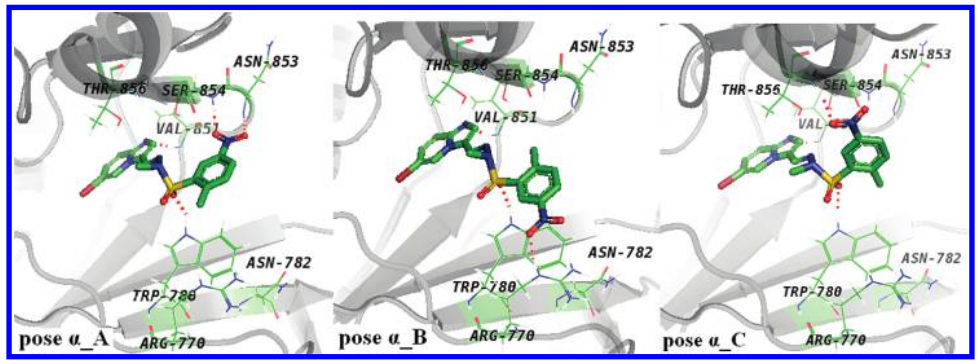

Figure 7. Three lowest docked energy structures in PI3Kα obtained from docking PIK-75 to the sixth cluster representative conformation extracted by the average-linkage clustering algorithm. Pose α_A, pose α_B, and pose α_C are shown from left to right. Green, red, blue, and brownish red represent carbon, oxygen, nitrogen, and bromine, respectively. Hydrogen bonds are red dashes.

The two predicted poses in the two best docking experiments are the same too. We refer to the two structures with two poses of PIK-75 in the top two ranked clusters as pose γ_A and pose γ_B.

*3.3.3. Predicted Docked Poses of PIK-75 for PI3K*α. The three docked poses of PIK-75 for PI3Kα in the top ranked clusters are shown in Figure 7. The NH of Val851 forms the conserved hydrogen with the nitrogen atom of the imidazole in PIK-75. Vulpetti and Bosotti[54] divide the ATP pocket into five regions: adenine, sugar, phosphate, buried, and solvent accessible. The conserved lipophilic adenine region of PI3Kα is made up of Ile800, Ile848, Val850, Val851, Met922, Phe930, and Ile932 and accommodates the flat 6-bromine imidazo[1,2-*a*]pyridine ring of PIK-75. There is a T-shaped contact between the aromatic rings of Tyr836 in PI3Kα and imidazo[1,2-*a*]pyridine ring of PIK-75, which agrees with Frédérick and Denny's observation.[18] The pyrazole NH of Trp780 forms a hydrogen bond with the oxygen atom of the sulfonyl group in PIK-75 as shown in Figure 7. The hydrogen bond increases the ligand binding affinity. In the three predicted poses of PIK-75, the 2-methyl-5-nitrophenyl group extends to three different directions. In the pose α_A-bound PI3Kα, the nitro moiety of PIK-75 has two hydrogen-bond arms with the backbone of Ser854 and Asn853. The Asn853 in PI3Kα corresponds to the Asp884 in PI3Kγ. The interaction between the Asp884 in PI3Kγ and the nitro moiety gets higher electrostatic energy, so there is no similar ligand orientation for PIK-75 with PI3Kγ. In the pose α_B-bound PI3Kα, the nitro moiety of PIK-75 is poised to make a hydrogen bond to Arg770. In the pose α_C-bound PI3Kα, the nitro moiety of PIK-75 forms a hydrogen bond with the residue Thr856.

3.3.4. Predicted Docked Poses of PIK-75 for PI3Kγ. The two docked poses of PIK-75 for PI3Kγ in the top ranked clusters are shown in Figure 8. The NH of Val882 forms the conserved hydrogen with the nitrogen atom of the imidazole of PIK-75. The conserved hydrophobic adenine region of PI3Kγ consists of residues Ile831, Ile881, Met804, Ile879, Val882, Ile963, Met953, Phe961, and Ala885 and accommodates the flat 6-bromine imidazo[1,2-*a*]pyridine ring of PIK-75. There is a T-shaped contact between the aromatic rings of Tyr867 and the imidazo[1,2-*a*]pyridine ring of PIK-75. In the two PI3Kγ complexes with two poses of PIK-75, the backbone NH in Thr887 is in close proximity to the ligand as shown in Figure 8. Two oxygen atoms and one nitrogen atom in the nitro moiety of PIK-75 are all sp^2 hybridized. The lone-pair direction of the two oxygen atoms

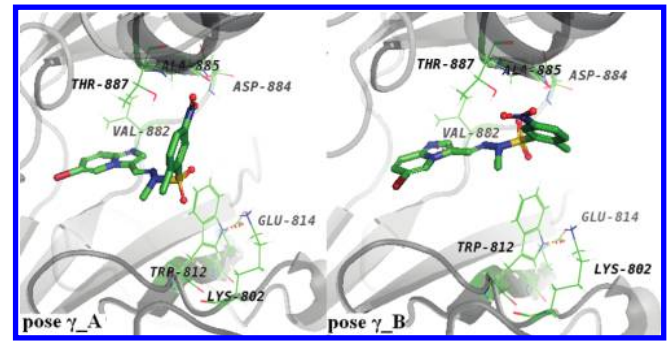

Figure 8. Two lowest docked energy structures in PI3Kγ obtained from docking PIK-75 to the third cluster representative conformation extracted by the average-linkage clustering algorithm: pose γ_A (left) and pose γ_B (right). Green, red, blue, and brownish red represent carbon, oxygen, nitrogen, and bromine, respectively. Hydrogen bonds are red dashes.

is in the plane of the nitro moiety. In the pose γ_A-bound PI3Kγ, while two oxygen atoms in the nitro moiety are located only 2.037 and 2.497 Å from the NH of Thr887, the deviation of the donor−acceptor axis from the closest lone-pair direction at the oxygen atom is as large as 80.3° and 75.4°, respectively. Therefore, no hydrogen bond between the ligand and the Thr887 exists for this pose. In the pose γ_ B-bound PI3Kγ, there is no hydrogen bond between Thr887 and the ligand either. The deviation of the donor−acceptor axis from the closest lone-pair direction at the oxygen atom is as large as 49.0° and 52.6°, although two oxygen atoms in the nitro moiety are located only 2.153 and 2.168 Å away from the NH of Thr887, respectively. However, the hydrogen bond between Thr887 and the nitro moiety was observed immediately after the molecular dynamics simulation began by adjusting the rotatable bond, which will be discussed in section 3.4. The pose γ_B orientes along the short peptide linking the two lobes, which makes the van der Waals energy lower.

3.3.5. Binding Free Energy Calculation. The binding free energy from docking experiments and energy decomposition by Autodock single-point energy calculation was analyzed and listed in Table 4. The energy in the third column is determined from docking experiments, calculated by interpolation of the sum of van der Waals, hydrogen-bond, desolvation, and electrostatic energies by precalculated grid maps. The AutoDock single-point score including electrostatic, hydrogen bond, van der Waals, desolvation, and torsion energies is calculated directly from the force field function. The difference in the energies among the mean

Table 4. Binding Free Energy (kcal mol^{-1}) from Docking Experiments and Energy Decomposition by Autodock Single-Point Energy Calculation

receptor	ligand	binding free energy by docking	binding free energy by single point score					
			total	electrostatic	hydrogen bond	van der Waals	desolvation	torsion
PI3Kα	α_A	−6.58	−9.6008	−0.3606	−2.1276	−10.5651	1.9611	1.4915
PI3Kα	α_B	−6.36	−9.3773	−0.8620	−1.5171	−10.1544	1.6645	1.4915
PI3Kα	α_C	−6.00	−8.5424	−0.3634	−1.3837	−10.1758	1.8890	1.4915
PI3Kγ	γ_A	−5.72	−8.4203	−0.6171	−0.9550	−9.9482	1.6085	1.4915
PI3Kγ	γ_B	−5.62	−8.6982	−0.3285	−1.0494	−10.7748	1.9630	1.4915

energies of the five best docked clusters is less than the standard deviation of the AutoDock force field, 2.1 kcal mol^{-1}. In addition to the standard error from the docking, the high predicted binding free energy, compared to the value from the real experiments listed in Table 2, comes from the not fully minimized complex, which only permits a coarse energy evaluation. The binding free energy of pose γ_B is lower than pose γ_A by single-point analysis. It is obvious that the van der Waals interaction is dominant to stabilize pose γ_B.

3.3.6. Specificity Analysis. From the docking studies described above, we conclude that residues Trp780 and Asn782 play an important role in conferring the inhibitor specificity between the two PI3K isoforms. In the structure of PI3Kγ there is a stable hydrogen bond between the pyrazole NH of Trp812 and Glu814 (as shown in Figures 3 and 4), which is observed throughout the LY294002-bound PI3Kγ simulation. However, the equivalent residues at these positions in PI3Kα, Trp780, and Asn782 do not form a hydrogen bond. Thus, in the PI3Kα structure, there is a chance for the free pyrazole NH of Trp780 to form a hydrogen bond with the oxygen atom of the sulfonyl group atom in PIK-75 as shown in Figure 7, while in the structure of PI3Kγ, Trp812 does not have this opportunity. In Frédérick and Denny's work[18] the homology model is based on the PI3Kγ crystal structure, so the orientation of Trp780 in the homology model of PI3Kα is the same as Trp812 in PI3Kγ. Then they have not discovered Trp780 for the selectivity.

Trp780 and Asn782 are not located in the highly conserved adenine, sugar, or phosphate regions but in the solvent-accessible region of the ATP binding pocket, which agrees with Vulpetti and Roberta's summary[54] about kinase pocket residues, that is, the solvent-accessible region can be exploited to increase the binding affinity. In the predicted PI3Kα and PI3Kγ complexes the ligands do not occupy the sugar, phosphate, and buried regions.

The predicted poses of PIK-75 and the coarse docking energy analysis suggest that the structure of a possible effective pharmacophore model for PI3Kα inhibitors should have the following features. In addition to the polar interaction of the critical hydrogen bond with the backbone of residue Val851, a flat aromatic scaffold should fit the lipophilic adenine region of the ATP-binding pocket. The hydrogen bonds between the possible sulfonic group or other groups with similar characteristics and Trp780 are necessary to increase the binding affinity. More hydrogen bonds between a group such as a nitro moiety and the receptor will help lock the ligand in the pocket. This pharmacophore model might provide helpful information for developing high-affinity inhibitors and lead optimization.

The docking results qualitatively explain the selectivity between the two PI3K isoforms. The predicted complexes should be solved in explicit waters by molecular dynamics simulation to check if the structures are stable.

3.4. Dynamics Analysis of Receptor−ligand Interaction in Aqueous Solution. The solvent effect on the ligands and kinases and the potential ligand-induced conformational changes are not fully taken into account in the docking experiments. Therefore, we simulated our predicted ligand-bound complex structures to check if they are stable in aqueous solution and if any induced fit takes place.

The system composition, periodic image distance, as well as total simulation time in each simulated system are listed

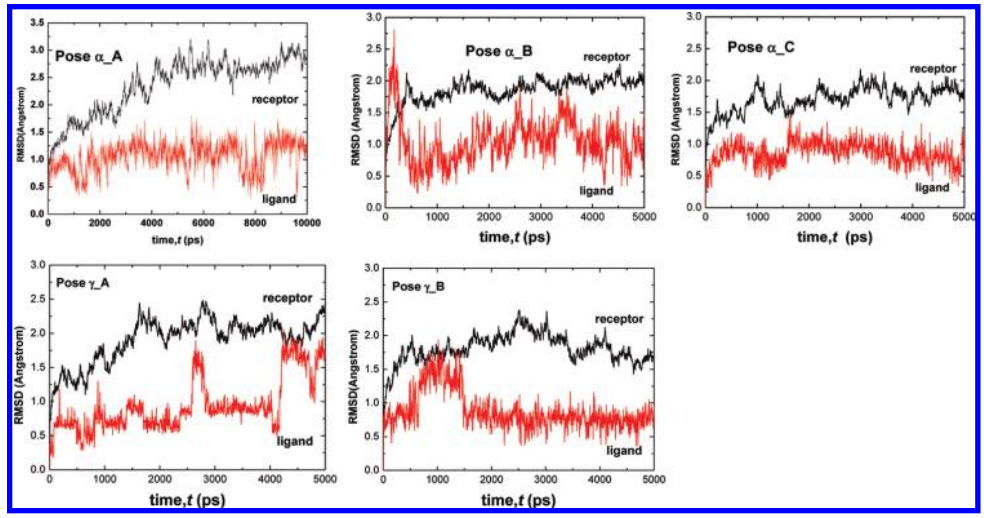

Figure 9. rmsd of Cα of the receptor and the heavy atoms in the ligand (black and red lines, respectively) of the pose α_A-, pose α_B-, and pose α_C-bound PI3Kαs and the pose γ_A- and pose γ_B-bound PI3Kγs as a function of the simulation time.

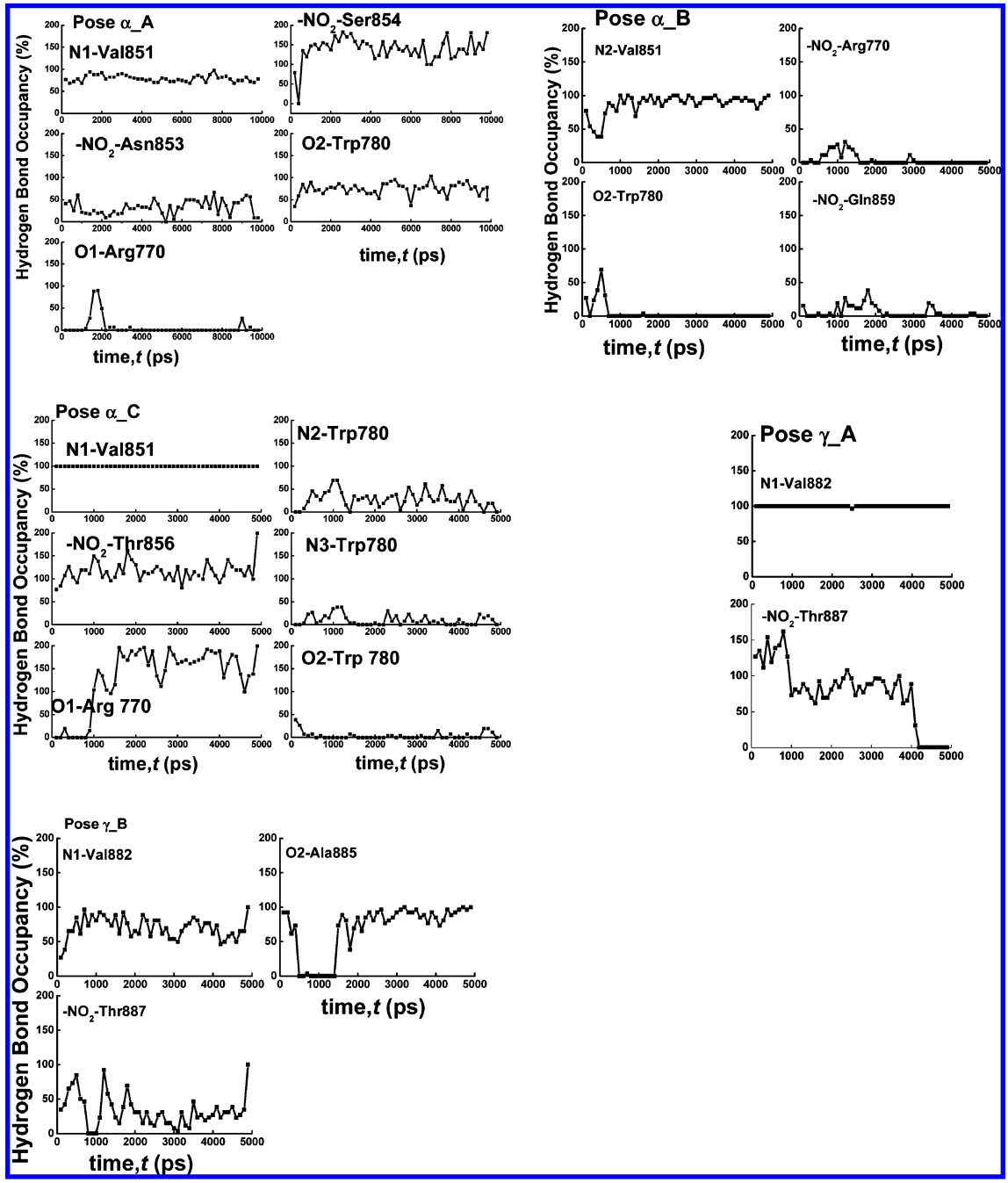

Figure 10. Hydrogen-bond occupancy analysis for the interaction between the ligands and the receptors in the pose α_A-, pose α_B-, and pose α_C-bound PI3Kαs and the pose γ_A- and pose γ_B-bound PI3Kγs as a function of the simulation time.

in Table 1. The rmsds of the receptors and ligands are analyzed to assess the degree of the conformation drift in Figure 9. The key hinge hydrogen bonds between the ligand and Val851 in PI3Kα or Val882 in PI3Kγ in each simulation were stable as shown in Figure 10.

In the simulation of the pose α_A-bound PI3Kα, the rmsd of the Cα of the receptor is stable after ~5 ns. The ligand-induced effect took place at the binding site, and the P-loop moved toward the inside of the ATP-binding pocket in the first 5 ns of the simulation. The hydrogen bonds between the nitro moiety in PIK-75 and Asn853, the nitro moiety in PIK-75 and Ser854, one oxygen atom of the sulfonyl group, and Trp780 remained stable during the 10 ns simulation. The other oxygen atom in the sulfonyl group formed hydrogen bonds with Arg770 occasionally.

In the pose α_B-bound PI3Kα, the hydrogen bond between the nitro moiety and Arg770 in the initial simulation structure broke within a very short time and the nitro moiety formed a hydrogen bond with Gln859 occasionally. The hydrogen bond between the oxygen of the sulfonyl group and Trp780 broke within 600 ps. The solvent affects the stability of the hydrogen bond between the nitro moiety of the PIK-75 and Arg770. Furthermore, because Trp780 and Arg770 are located in two different β sheets connecting the P-loop, the movement of the flexible P-loop will break the two hydrogen bonds easily.

In the pose α_C-bound PI3Kα, both receptor and ligand were stable. The hydrogen bond between the nitro moiety and residue Thr856 in the initial structures remained stable. Atom O1 formed stable hydrogen bonds with Arg770 after

~1 ns, which helped Trp780 lock the ligand in the ATP binding pocket. The N2, N3, and O2 atoms competed to form hydrogen bonds with residue Trp780 (as shown in Figure 10), which provided flexibility for the Trp780 to interact with the ligand. The corresponding residue of Arg770 in PI3Kγ is Lys 802. Arginine has both a larger pK_R and a longer side chain than lysine, which makes it more likely for Arg770 to form hydrogen bonds with the middle part of the ligand than in the case of Lys 802 in PI3Kγ; therefore, Arg770 is another possible factor for the selectivity.

In the pose γ_A-bound PI3Kγ, the nitro moiety formed hydrogen bonds with Thr887 immediately after the simulation began but broke after 4 ns. This largest conformational transition can be found in the rmsd shown in Figure 9.

In the pose γ_B-bound PI3Kγ, the receptor remained stable throughout the simulation and the ligand became stable after the fluctuation in the beginning. The hydrogen bond between Thr887 and the nitro moiety formed immediately after the simulation began. One oxygen atom of the sulfonyl group formed stable hydrogen bonds with the NH of the backbone of Ala885 after the fluctuation in the first 1.5 ns as shown in Figure 10. Both the van der Waals interaction and the hydrogen bonds keep the structure stable.

In summary, pose α_A, pose α_C, and pose γ_B are stable inhibitor orientations in the MD simulations of the complexes. The hydrogen bonds between the ligand and Trp780 and between the ligand and Arg770 provide stability in addition to the hydrogen bond with the hinge residue. The simulation shows that residue Arg770 in PI3Kα is another possible key residue to confer selectivity.

The kinase domains are truncated from the catalytic subunit of PI3Ks. The PI3K kinase family is located near the cellular membrane and has close interaction with membrane lipids; thus, the real environment for PI3Ks is more complicated. The whole catalytic subunit and the regulatory subunit with a more accurate environment should be involved in future molecular dynamics simulation.

4. CONCLUSION

The PI3Ks, in particular PI3Kα, are promising targets for anticancer therapeutics. Selectively targeting the isoforms of the PI3K family is required in order to decrease the side effects of the therapeutics. We used docking and molecular dynamics simulation methods to explore the structural basis that confers the selectivity between PI3Kα and PI3Kγ. Protein flexibility was taken into account in molecular docking by constructing an ensemble of cluster representative receptor conformations extracted from molecular dynamics simulation. Our study confirms that there is a possibility for the ligand to discriminate between PI3Kα and PI3Kγ. Residues Trp780, Asn782, and Arg770 in PI3Kα were identified as enabling selective inhibition, and this was confirmed by our MD simulations. This work is likely to provide important insights into strategies for the discovery of more promising compounds to target PI3Kα.

ACKNOWLEDGMENT

We are very grateful to the reviewer for the comments and recommendations. We thank S. K. Dutta for suggestions to improve the manuscript. We thank Yan Ji and Yongle Li for discussion. This work was partially supported by grants from the National Science Foundation of China (grant no. 20773060) and National Basic Research Program of China (grant no. 2004CB719901).

Supporting Information Available: Atomic types and partial atomic charges of PIK-75 and LY294002 and missing force field parameters for LY294002 and PIK-75. This material is available free of charge via the Internet at http://pubs.acs.org.

REFERENCES AND NOTES

(1) Stein, R. C.; Waterfield, M. D. PI3-kinase inhibition: a target for drug development. *Mol. Med. Today* **2000**, *6*, 347–358.
(2) Fruman, D. A.; Meyers, R. E.; Cantley, L. C. Phosphoinositide Kinases. *Annu. Rev. Biochem.* **1998**, *67*, 481–507.
(3) Rodriguez-Viciana, P.; Warne, P. H.; Dhand, R.; Vanhaesebroeck, B.; Gout, I.; Fry, M. J.; Waterfield, M. D.; Downward, J. Phosphatidylinositol-3-OH kinase direct target of Ras. *Nature* **1994**, *370*, 527–532.
(4) Vivanco, I.; Sawyers, C. L. The phosphatidylinositol 3-Kinase-AKT pathway in human cancer. *Nat. Rev. Cancer* **2002**, *2*, 489–501.
(5) Vanhaesebroeck, B.; Waterfield, M. D. Signaling by Distinct Classes of Phosphoinositide 3-Kinases. *Exp. Cell Res.* **1999**, *253*, 239–254.
(6) Domin, J.; Waterfield, M. D. Using structure to define the function of phosphoinositide 3-kinase family members. *FEBS Lett.* **1997**, *410*, 91–95.
(7) Chang, H. W.; Aoki, M.; Fruman, D.; Auger, K. R.; Bellacosa, A.; Tsichlis, P. N.; Cantley, L. C.; Roberts, T. M.; Vogt, P. K. Transformation of Chicken Cells by the Gene Encoding the Catalytic Subunit of PI 3-Kinase. *Science* **1997**, *276*, 1848–1850.
(8) Li, J.; Yen, C.; Liaw, D.; Podsypanina, K.; Bose, S.; Wang, S. I.; Puc, J.; Miliaresis, C.; Rodgers, L.; McCombie, R.; Bigner, S. H.; Giovanella, B. C.; Ittmann, M.; Tycko, B.; Hibshoosh, H.; Wigler, M. H.; Parsons, R. PTEN a Putative Protein Tyrosine Phosphatase Gene Mutated in Human Brain, Breast, and Prostate Cancer. *Science* **1997**, *275*, 1943–1947.
(9) Sansal, I.; Sellers, W. R. The Biology and Clinical Relevance of the PTEN Tumor Suppressor Pathway. *J. Clin. Oncol.* **2004**, *22*, 2954–2963.
(10) Steck, P. A.; Pershouse, M. A.; Jasser, S. A.; Yung, W. K. A.; Lin, H.; Ligon, A. H.; Langford, L. A.; Baumgard, M. L.; Hattier, T.; Davis, T.; Frye, C.; Hu, R.; Swedlund, B.; Teng, D. H. R.; Tavtigian, S. V. Identification of a candidate tumour suppressor gene, MMAC1, at chromosome 10q23.3 that is mutated in multiple advanced cancers. *Nat. Genet.* **1997**, *15*, 356–362.
(11) Samuels, Y.; Diaz Jr, L. A.; Schmidt-Kittler, O.; Cummins, J. M.; DeLong, L.; Cheong, I.; Rago, C.; Huso, D. L.; Lengauer, C.; Kinzler, K. W.; Vogelstein, B.; Velculescu, V. E. Mutant PIK3CA promotes cell growth and invasion of human cancer cells. *Cancer Cell* **2005**, *7*, 561–573.
(12) Samuels, Y.; Wang, Z.; Bardelli, A.; Silliman, N.; Ptak, J.; Szabo, S.; Yan, H.; Gazdar, A.; Powell, S. M.; Riggins, G. J.; Willson, J. K. V.; Markowitz, S.; Kinzler, K. W.; Vogelstein, B.; Velculescu, V. E. High Frequency of Mutations of the PIK3CA Gene in Human Cancers. *Science* **2004**, *304*, 554.
(13) Marone, R.; Cmiljanovic, V.; Giese, B.; Wymann, M. P. Targeting phosphoinositide 3-kinase--Moving towards therapy. *BBA* **2008**, *1784*, 159–185.
(14) Knight, Z. A.; Gonzalez, B.; Feldman, M. E.; Zunder, E. R.; Goldenberg, D. D.; Williams, O.; Loewith, R.; Stokoe, D.; Balla, A.; Toth, B.; Balla, T.; Weiss, W. A.; Williams, R. L.; Shokat, K. M. A Pharmacological Map of the PI3-K Family Defines a Role for p110α in Insulin Signaling. *Cell* **2006**, *125*, 733–747.
(15) Knight, Z. A.; Shokat, K. M. Chemically targeting the PI3K family. *Biochem. Soc. Trans.* **2007**, *35*, 245–249.
(16) Amzel, L. M.; Huang, C.-H.; Mandelker, D.; Lengauer, C.; Gabelli, S. B.; Vogelstein, B. Structural comparisons of class I phosphoinositide 3-kinases. *Nat. Rev. Cancer* **2008**, *8*, 665–669.
(17) Zvelebil, M. J.; Waterfield, M. D.; Shuttleworth, S. J. Structural analysis of PI3-kinase isoforms: Identification of residues enabling selective inhibition by small molecule ATP-competitive inhibitors. *Arch. Biochem. Biophys.* **2008**, *477*, 404–410.
(18) Frederick, R.; Denny, W. A. Phosphoinositide-3-kinases (PI3Ks): Combined Comparative Modeling and 3D-QSAR to Rationalize the Inhibition of p110α. *J. Chem. Inf. Model.* **2008**, *48*, 629–638.
(19) Cheng, L. S.; Amaro, R. E.; Xu, D.; Li, W. W.; Arzberger, P. W.; McCammon, J. A. Ensemble-Based Virtual Screening Reveals Potential Novel Antiviral Compounds for Avian Influenza Neuraminidase. *J. Med. Chem.* **2008**, *51*, 3878–3894.

(20) Carlson, H. A.; Masukawa, K. M.; Rubins, K.; Bushman, F. D.; Jorgensen, W. L.; Lins, R. D.; Briggs, J. M.; McCammon, J. A. Developing a dynamic pharmacophore model for HIV-1 integrase. *J. Med. Chem.* **2000**, *43* (11), 2100–2114.
(21) Kua, J.; Zhang, Y.; McCammon, J. A. Studying enzyme binding specificity in acetylcholinesterase using a combined molecular dynamics and multiple docking approach. *J. Am. Chem. Soc.* **2002**, *124* (28), 8260–8267.
(22) Lin, J. H.; Perryman, A. L.; Schames, J. R.; McCammon, J. A. Computational drug design accommodating receptor flexibility: the relaxed complex scheme. *J. Am. Chem. Soc.* **2002**, *124* (20), 5632–5633.
(23) Cavasotto, C. N.; Abagyan, R. A. Protein flexibility in ligand docking and virtual screening to protein kinases. *J. Mol. Biol.* **2004**, *337* (1), 209–225.
(24) Cavasotto, C. N.; Kovacs, J. A.; Abagyan, R. A. Representing receptor flexibility in ligand docking through relevant normal modes. *J. Am. Chem. Soc.* **2005**, *127* (26), 9632–9640.
(25) Sherman, W.; Day, T.; Jacobson, M. P.; Friesner, R. A.; Farid, R. Novel procedure for modeling ligand/receptor induced fit effects. *J. Med. Chem.* **2006**, *49* (2), 534–553.
(26) Damm, K. L.; Carlson, H. A. Exploring experimental sources of multiple protein conformations in structure-based drug design. *J. Am. Chem. Soc.* **2007**, *129* (26), 8225–8235.
(27) Walker, E. H.; Pacold, M. E.; Perisic, O.; Stephens, L.; Hawkins, P. T.; Wymann, M. P.; Williams, R. L. Structural Determinants of Phosphoinositide 3-Kinase Inhibition by Wortmannin, LY294002, Quercetin, Myricetin, and Staurosporine. *Mol. Cell.* **2000**, *6*, 909–919.
(28) Apsel, B.; Blair, J. A.; Gonzalez, B.; Nazif, T. M.; Feldman, M. E.; Aizenstein, B.; Hoffman, R.; Williams, R. L.; Shokat, K. M.; Knight, Z. A. Targeted polypharmacology: discovery of dual inhibitors of tyrosine and phosphoinositide kinases. *Nat. Chem. Biol.* **2008**, *4*, 691–699.
(29) Huang, C.-H.; Mandelker, D.; Schmidt-Kittler, O.; Samuels, Y.; Velculescu, V. E.; Kinzler, K. W.; Vogelstein, B.; Gabelli, S. B.; Amzel, L. M. The Structure of a Human p110α/p85α Complex Elucidates the Effects of Oncogenic PI3Kα Mutations. *Science* **2007**, *318*, 1744–1748.
(30) Hayakawa, M.; Kawaguchi, K.-i.; Kaizawa, H.; Koizumi, T.; Ohishi, T.; Yamano, M.; Okada, M.; Ohta, M.; Tsukamoto, S.-i.; Raynaud, F. I.; Parker, P.; Workman, P.; Waterfield, M. D. Synthesis and biological evaluation of sulfonylhydrazone-substituted imidazo[1,2-a]pyridines as novel PI3 kinase p110[alpha] inhibitors. *Bioorgan. Med. Chem.* **2007**, *15*, 5837–5844.
(31) Sali, A.; Blundell, T. L. Comparative Protein Modelling by Satisfaction of Spatial Restraints. *J. Mol. Biol.* **1993**, *234*, 779–815.
(32) Andrάs, F.; Richard Kinh Gian, D.; Andrej, S. Modeling of loops in protein structures. *Protein Sci.* **2000**, *9*, 1753–1773.
(33) *Gaussian 03*, Revision D.01; Gaussian, Inc.: Wallingford, CT, 2004.
(34) Garrett, M. M.; David, S. G.; Robert, S. H.; Ruth, H.; William, E. H.; Richard, K. B.; Arthur, J. O. Automated docking using a Lamarckian genetic algorithm and an empirical binding free energy function. *J. Comput. Chem.* **1998**, *19*, 1639–1662.
(35) Ruth, H.; Garrett, M. M.; Arthur, J. O.; David, S. G. A semiempirical free energy force field with charge-based desolvation. *J. Comput. Chem.* **2007**, *28*, 1145–1152.
(36) Michel, F. Sanner. Python: A Programming Language for Software Integration and Development. *J. Mol. Graph. Model.* **1999**, *17*, 57–61.
(37) Gasteiger, J.; Marsili, M. Iterative partial equalization of orbital electronegativity--a rapid access to atomic charges. *Tetrahedron* **1980**, *36* (22), 3219–3228.
(38) Case, D. A.; Darden, T. A.; Cheatham, T. E., III; Simmerling, C. L.; Wang, J.; Duke, R. E.; Luo, R.; Crowley, M.; Walker, R. C.; Zhang, W.; Merz, K. M.; Wang, B.; Hayik, S.; Roitberg, A.; Seabra, G.; Kolossváry, I.; Wong, K. F.; Paesani, F.; Vanicek, J.; Wu, X.; Brozell, S. R.; Steinbrecher, T.; Gohlke, H.; Yang, L.; Tan, C.; Mongan, J.; Hornak, V.; Cui, G.; Mathews, D. H. Seetin, M. G.; Sagui, C.; Babin, V.; Kollman, P. A. *AMBER 10*; University of California: San Francisco, 2008.
(39) Viktor, H.; Robert, A.; Asim, O.; Bentley, S.; Adrian, R.; Carlos, S. Comparison of multiple Amber force fields and development of improved protein backbone parameters. *Proteins* **2006**, *65*, 712–725.
(40) Junmei, W.; Romain, M. W.; James, W. C.; Peter, A. K.; David, A. C. Development and testing of a general amber force field. *J. Comput. Chem.* **2004**, *25*, 1157–1174.
(41) Jakalian, A.; Bush, B. L.; Jack, D. B.; Bayly, C. I. Fast, efficient generation of high-quality atomic charges. AM1-BCC model: I. Method. *J. Comput. Chem.* **2000**, *21*, 132–146.
(42) Jakalian, A.; Jack, D. B.; Bayly, C. I. Fast, efficient generation of high-quality atomic charges. AM1-BCC model: II. Parameterization and Validation. *J. Comput. Chem.* **2002**, *23*, 1623–1641.
(43) Darden, T.; York, D.; Pedersen, L. Particle mesh Ewald: An N·log(N) method for Ewald sums in large systems. *J. Chem. Phys.* **1993**, *98*, 10089–10092.
(44) Pastor, R. W.; Brooks, B. R.; Szabo, A. An analysis of the accuracy of Langevin and molecular dynamics algorithms. *Mol. Phys.* **1988**, *65*, 1409–1419.
(45) Loncharich, R. J.; Brooks, B. R.; Pastor, R. W. Langevin dynamics of peptides: The frictional dependence of isomerization rates of N-actylananyl-N'-methylamide. *Biopolymers* **1992**, *32*, 523–535.
(46) Berendsen, H. J. C.; Postma, J. P. M.; van Gunsteren, W. F.; DiNola, A.; Haak, J. R. Molecular dynamics with coupling to an external bath. *J. Chem. Phys.* **1984**, *81*, 3684–3690.
(47) Ryckaert, J.-P.; Ciccotti, G.; Berendsen, H. J. C. Numerical integration of the cartesian equations of motion of a system with constraints: molecular dynamics of n-alkanes. *J. Comput. Phys.* **1977**, *23*, 327–341.
(48) Miyamoto, S.; Kollman, P. A. Settle: An analytical version of the SHAKE and RATTLE algorithm for rigid water models. *J. Comput. Chem.* **1992**, *13*, 952–962.
(49) Kendall, J. D.; Rewcastle, G. W.; Frederick, R.; Mawson, C.; Denny, W. A.; Marshall, E. S.; Baguley, B. C.; Chaussade, C.; Jackson, S. P.; Shepherd, P. R. Synthesis, biological evaluation and molecular modelling of sulfonohydrazides as selective PI3K p110α inhibitors. *Bioorg. Med. Chem.* **2007**, *15*, 7677–7687.
(50) Brunger, A. T.; Adams, P. D.; Clore, G. M.; DeLano, W. L.; Gros, P.; Grosse-Kunstleve, R. W.; Jiang, J. S.; Kuszewski, J.; Nilges, M.; Pannu, N. S.; Read, R. J.; Rice, L. M.; Simonson, T.; Warren, G. L. Crystallography & NMR system: A new software suite for macromolecular structure determination. *Acta Crystallogr., Sect. D* **1998**, *54*, 905–921.
(51) Camps, M.; Ruckle, T.; Ji, H.; Ardissone, V.; Rintelen, F.; Shaw, J.; Ferrandi, C.; Chabert, C.; Gillieron, C.; Francon, B.; Martin, T.; Gretener, D.; Perrin, D.; Leroy, D.; Vitte, P.-A.; Hirsch, E.; Wymann, M. P.; Cirillo, R.; Schwarz, M. K.; Rommel, C. Blockade of PI3Kγ suppresses joint inflammation and damage in mouse models of rheumatoid arthritis. *Nat. Med.* **2005**, *11*, 936–943.
(52) Yung-Chi, C.; Prusoff, W. H. Relationship between the inhibition constant (KI) and the concentration of inhibitor which causes 50% inhibition (I50) of an enzymatic reaction. *Biochem. Pharmacol.* **1973**, *22*, 3099–3108.
(53) Chaussade, C.; Rewcastle, G. W.; Kendall, J. D.; Denny, W. A.; Cho, K.; Gronning, L. M.; Chong, M. L.; Anagnostou, S. H.; Jackson, S. P.; Daniele, N.; Shepherd, P. R. Evidence for functional redundancy of class IA PI3K isoforms in insulin signalling. *Biochem. J.* **2007**, *404*, 449–458.
(54) Vulpetti, A.; Bosotti, R. Sequence and structural analysis of kinase ATP pocket residues. *Il Farmaco* **2004**, *59*, 759–765.

CI900175N